Chaotic solutions found in the gravity model of network transport

Hajime Koike [*]
Graduate School of Informatics, Kyoto University, Kyoto 606-8501, Japan

Hideki Takayasu and Misako Takayasu [†]
School of Computing, Institute of Science Tokyo, Yokohama 226-8502, Japan

(Received 24 October 2024; accepted 20 April 2025; published 5 June 2025)

The gravity model is a mathematical model that applies Newton's universal law of gravitation to socioeconomic transport phenomena and has been widely used to describe world trade, intercity traffic flows, and business transactions for several decades. However, its strong nonlinearity and diverse network topology make a theoretical analysis difficult, and only a short history of studies on its stability exists. In this study, the stability of gravity models defined on networks with few nodes is analyzed in detail using numerical simulations. It was found that, other than the previously known transition of stationary solutions from a unique diffusion solution to multiple localized solutions, parameter regions exist where periodic solutions with the same repeated motions and chaotic solutions with no periods are realized. The smallest network with chaotic solutions was found to be a ring with seven nodes, which produced a new type of chaotic solution in the form of a mixture of right and left periodic solutions.

DOI: 10.1103/PhysRevResearch.7.023232

I. INTRODUCTION

Transport in socioeconomic systems is ubiquitousand found in various spatiotemporal scales, such as the movement and exchange of money and goods, measured at the scale of intra-cities, inter-cities, and countries. Typically, the gravity law is used as a model of fluxes in these transport systems, such as world trade [1,2], population movement [3–7], traffic [8–11], human mobility [12,13], and business transactions [14]. With technological advancements, the types and scales of transportation have continuously expanded. Furthermore, the acquisition of big data has made it possible to observe interactions between entities at a scale that is more microscopic than ever before. As a result, the scope of application for gravity laws continues to expand even today.

Owing to this ubiquity, the gravity law has been a long-standing research topic in social science and economics. Many studies have been done on the empirical validation of the gravity law [4–7,9–14] or deriving the gravity law theoretically [2,15,16], whereas very few studies have been conducted on the stability of transport systems driven by the gravity law. Nevertheless, the stability of the transport systems governed by the gravity law remains a profound subject, because the aforementioned examples of such systems are fundamental components of our society. Studies on the stability of the transport systems are desired from both the theoretical understanding of them and the practical need to control them.

To address this problem explicitly, one approach involves interpreting the transport by the gravity law as nonlinear transport on networks. The gravity law defined on the edges of the network serves as a nonlinear function to determine the interaction flux, because the flux depends not only on the size of the source site but also on the size of the target site. Along this direction, a model known as a "gravity interaction model" [17–19] acted as a working model of an open system of gravity law transport in investigating the role played by the combination of network topology and nonlinearity in the stability of the state.

To clarify the role of gravity interaction in stability, a basic question arises: What is the possible nonlinear behavior, such as oscillatory states and chaotic states? The transition from a diffusive state to a localized state is reported in Refs. [17,18]. Recently, our model study revealed hysteresis in a three-node system of gravity law transport [19]. These studies focused only on the stability of the fixed points; however, possibilities exist for other types of solutions.

In this paper, we study the gravity interaction model and show the phase diagram of the model on rings—one of the simplest network structures for investigating behaviors beyond fixed points—to explore diverse solutions. In particular, we found a chaotic region in the localized phase for the first time, even in small networks, such as ring networks with only seven nodes. We show strange attractors in such cases and elucidate the mechanism of the chaotic solution from the perspective of the stability of symmetric localized fixed points. We find that such chaotic behavior occurs for $n \geqslant 7$

[*]Contact author: hajimekoike@outlook.jp
[†]Contact author: takayasu@comp.isct.ac.jp

Published by the American Physical Society under the terms of the Creative Commons Attribution 4.0 International license. Further distribution of this work must maintain attribution to the author(s) and the published article's title, journal citation, and DOI.

nodes in the ring network and, finally, discuss the role of dissipation.

II. MODEL

The equation of the gravity law is

$$f_{ij} \propto A_{ij} \frac{S_i^\alpha S_j^\beta}{d_{ij}^\delta}, \tag{1}$$

where f_{ij} is the flux from nodes i to j, A_{ij} is the binary adjacency matrix of the network, S_i, S_j are the sizes of i and j, and d_{ij} is the distances between i and j, for some fixed parameters $\alpha, \beta, \delta \geqslant 0$. In the classical cases of world trade [1] and human movement [4], the values of α and β are $\alpha = \beta = 1$, and δ is either $\delta = 1$ [4] or 2 [1]. More recent studies of microscopic data revealed a further development of the gravity law. In the case of intra-city human mobility, the distance decay exponent δ is reported as 0.57 [13], and its value is expected to be close to 0 in the business relations [20]. Other studies show that the distance decay exponent δ temporally varies due to globalization and economic changes [21,22].

Gravity law (1) provides the functional form of the flux as follows:

$$f_{ij} = \frac{A_{ij} d_{ij}^{-\delta} S_j^\beta}{\sum_k A_{ik} d_{ik}^{-\delta} S_k^\beta} D S_i^\alpha, \tag{2}$$

where D is a normalization factor. We call this "share interpretation," where the fraction corresponds to a share of node j, and the term DS_i^α corresponds to the total volume of outgoing flow from node i per unit-time. This representation is often referred to as the "singly constrained gravity model" [16] in transportation modeling literature. In this interpretation, we can see the roles of exponents α, β, and δ. The parameter α characterizes the nonlinearity of the total outflow, and the parameter β characterizes the nonlinearity of the inflow. In the case of thermal diffusion, $\alpha = 1$ and $\beta = 0$.

When we consider real transportation systems, the flow is often not conserved in the given network, and we need to introduce injection and dissipation. For example, international migration flow is not closed in the country network; the number of humans is changing due to birth and death in each country. Money flow is not closed in the firm-to-firm business network; money is injected into business firms from individuals, banks, or firms abroad, and dissipation occurs due to employees' salaries, taxes to the government, or payments to other countries. These examples illustrate the open nature of the network flow systems. Here, since we are discussing the microscopic basis of the macroscopic network transport of gravity law, it is natural to consider dissipation and injection.

By using this flux formula (2), it is natural to construct the equation of continuity as follows:

$$\dot{S}_j = D\left[\sum_i \frac{A_{ij} d_{ij}^{-\delta} S_j^\beta}{\sum_k A_{ik} d_{ik}^{-\delta} S_k^\beta} S_i^\alpha - S_j^\alpha\right] - \nu_j S_j^\alpha + F_j. \tag{3}$$

Here, the role of the dissipation parameter ν_j and injection constant F_j is to control the external interaction of flows. This is the general formulation of the gravity interaction model of network transport. For the business transaction, we can construct the model (3) of companies' annual sales from business transaction data consisting of approximately one million Japanese companies by considering the money flow between companies via transactions, with dissipation and injection [14,17]. It is possible to recover Zipf's law of the sales at $\alpha = 0.9, \beta = 0.3, \delta = 0, D = 1$, and $\nu_j = \nu = 0.1, F_j = F = 95\ \forall j$ [17]. This is intriguing because not only the underlying network structure but also nonlinearity exponents α and β are essential components to reproduce real sales distribution. For simplicity, we consider a special case of this gravity interaction model (3), where $\delta = 0$, $D = 1$, and uniform external interaction parameters $\nu_j = \nu, F_j = F\ \forall j$, and network topology is fixed over time. This parameter setting reduces the number of parameters drastically, but the model is still relevant for describing the real data of money flow in Japanese business networks [17].

We consider a ring network, where each node follows a simple, identical external interaction coupled with a gravity interaction. It is natural to assume bidirectional interactions because interactions do not comprise only unidirectional links in reality. Then, it is possible to formulate the time evolution of the size variables $x_j = S_j^\alpha / F$ for each node $j = 1, 2, \ldots, n$ as follows:

$$\dot{x}_j = \frac{x_j^\gamma}{x_{j-2}^\gamma + x_j^\gamma} x_{j-1} + \frac{x_j^\gamma}{x_j^\gamma + x_{j+2}^\gamma} x_{j+1} - x_j - \nu x_j + 1, \quad j = 1, 2, \ldots, n, \tag{4}$$

where γ denotes the parameter of the nonlinearity of the flux and ν denotes the dissipation coefficient controlling the external interaction with the outside of the network. The first three terms are couplings, and the last two terms are external interactions—that is, dissipation and injection. It is possible to recover the typical diffusion at $\gamma = 0$. Because all elements are identical, $\langle x(t) \rangle \equiv \frac{1}{n} \sum_j x_j(t)$ asymptotically converges to ν^{-1}, implying that the dynamics are confined to a plane in the phase space. In particular, the model (4) admits the uniform state $x_j = \nu^{-1}\ \forall j$ for any γ. Because we consider a ring network, our model has rotational and reflection symmetries. For the numerical integration, we used the fourth-order Runge-Kutta method with a fixed time step size of 0.01. For a different time step size (0.1, 0.005 for fourth-order Runge-Kutta method) and integration scheme (adaptive step size integration with Dormand-Prince method), we confirmed that the result behaves the same qualitatively. The initial state is uniformly sampled from $[\nu^{-1} - 1, \nu^{-1} + 1]$ in the case of $\nu < 1$, and $[\nu^{-1} - 0.1, \nu^{-1} + 0.1]$ in the case of $\nu \geqslant 1$, for each node of the ring network.

III. LOCALIZED SOLUTIONS: TYPICAL FOUR PHASES

The numerical result reveals that four phases exist in our model: (a) diffusive phase: the fixed point at $\gamma = 0$ (the uniform state $x_j = \nu^{-1}\ j = 1, 2, \ldots, n$) is stable, (b) first localized phase: the fixed point at $\gamma = 0$ becomes unstable and multiple localized fixed points become stable, (c) chaotic region: the localized fixed points change their stability and the periodic or chaotic trajectory becomes the attractor, and

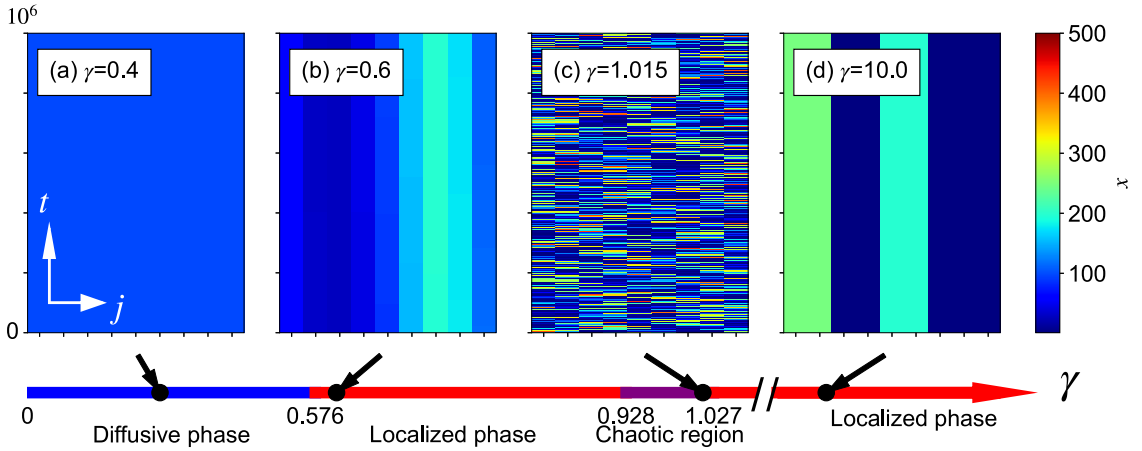


FIG. 1. Four phases of our model. Panels (a)-(d) show spatiotemporal patterns of the model's solution corresponding to four typical states. Horizontal and vertical axes represent space j (node positions aligned in a circular order of the ring network) and time t, respectively. Color indicates the state variable x. (a) Diffusive phase: The fixed point at $\gamma = 0$ is stable. (b) First localized phase: The fixed point at $\gamma = 0$ becomes unstable, and multiple localized fixed points emerge. (c) Chaotic region: The trajectory does not converge to a fixed point. Instead, it becomes periodic or chaotic. (d) Second localized phase: Multiple localized fixed points coexist.

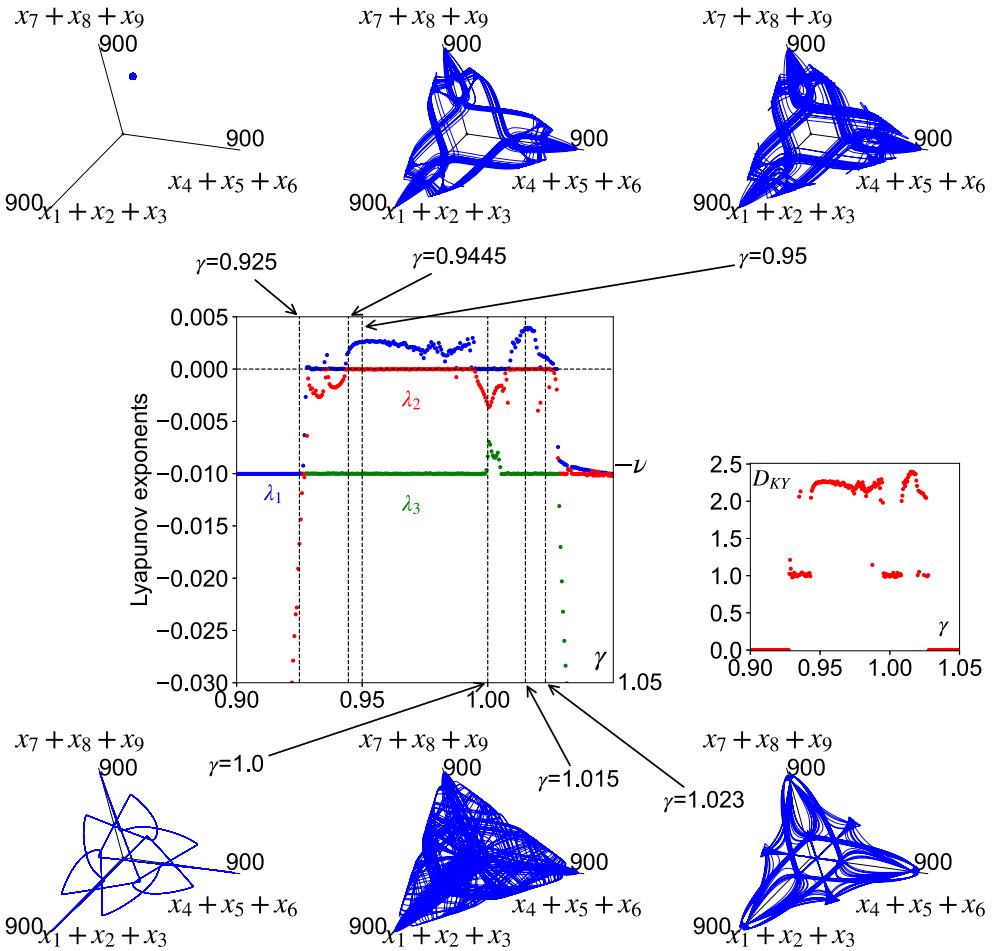


FIG. 2. Enlargement of the chaotic region. The center left panel shows the top three Lyapunov exponents λ_1(blue), λ_2(red), and λ_3(green) versus γ, whereas the center right panel shows the Kaplan-Yorke dimension D_{KY} calculated from the Lyapunov spectrum. The top and bottom panels show attractors for different values of γ across the chaotic region. Dissipation ν is fixed to 0.01. Attractors are represented in three-dimensional space, with coordinate axes being $x_1 + x_2 + x_3$, $x_4 + x_5 + x_6$, and $x_7 + x_8 + x_9$. The top three attractors are obtained for $\gamma = 0.925$ (fixed point attractor), 0.9445 (strange attractor), and 0.95 (strange attractor), and the bottom three attractors are obtained for $\gamma = 1.0$ (torus attractor), $\gamma = 1.015$ (strange attractor), and 1.023 (strange attractor). The value of D_{KY} is up to 2.5 throughout the chaotic region, justifying the representation of attractors in three-dimensional space.

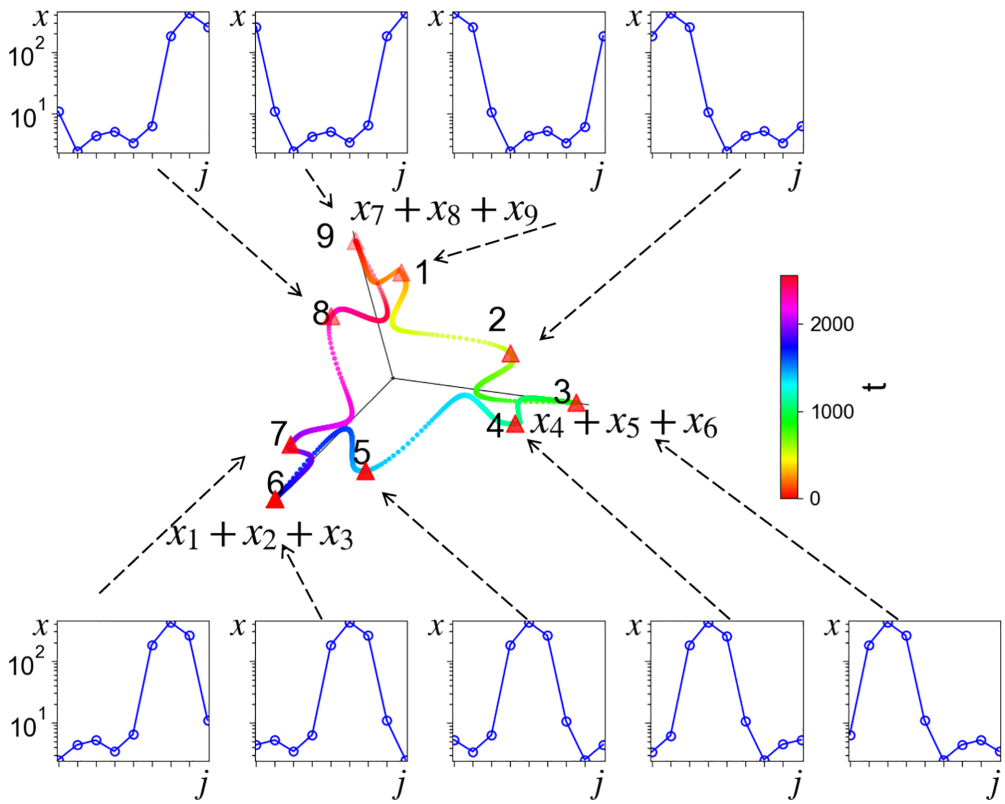


FIG. 3. Example of the attractor structure, obtained for $\gamma = 0.943$, in the vicinity of the left onset of chaos. A nine-dimensional trajectory is represented in three-dimensional space in the same manner as attractors in Fig. 2. The trajectory is traveling around nine saddle points (shown in the top and bottom panels, with horizontal and vertical axes being space j and value x, respectively) from 1, 2, . . ., 9 in the center panel.

(d) second localized phase: the localized fixed points become stable again. These four phases in Eq. (1) are shown in Fig. 1. The four panels show a 10^6 time-unit trajectory. The bifurcation point γ_c of the uniform state has been studied as the diffusion-localization transition point [17,18] and is approximately 0.576 for $\nu = 0.01$ for $n \to \infty$. The wave-like localized fixed points become stable at this bifurcation. Multiple localized fixed points exist owing to symmetry, and the state eventually converges on one of them depending on the initial state. In the localized phase, the wavelength of the localized fixed point is reduced by increasing γ. At certain values of γ, the fixed points become saddles, and the periodic trajectory traveling around these saddles becomes the attractor. This periodic trajectory becomes chaos at the left onset of the chaotic region. At the right onset of the chaos, the chaotic state becomes transient chaos, and eventually, the localized fixed points become stable again. In this second localized phase, the localized state consists of two waves of wavelength four, and in each wave there are two peak nodes [see Fig. 1(d)]. In this state, a main-stream structure [23] of flow exists; the two nodes at the peak of the wave are propelling each other, and the other nodes are being propelled only to the adjacent node which is nearer to the peak nodes. No further wavelength shortening occurs by increasing γ, because this state is stabilized by strong nonlinearity. The stability of the uniform state presents the characteristic wavelength as a function of γ, which confirms the above picture [24].

IV. CHAOTIC SOLUTIONS IN RING NETWORK

For the chaotic region, we calculated the Lyapunov exponents numerically. The calculation is based on the Shimada-Nagashima algorithm [25], with 1 time-unit re-orthogonalization, for a 10^5 time-unit trajectory after a 10^3 time-unit transient. The results are shown in the middle left panel of Fig. 2. The results did not change qualitatively for different transient and trajectory time lengths. This revealed the existence of periodic and chaotic regions for parameters ranging from approximately 0.928 to 1.027. The top and bottom panels show the attractors represented in three-dimensional space, with the axes being the sum of three adjacent nodes, namely, $x_1 + x_2 + x_3$, $x_4 + x_5 + x_6$, and $x_7 + x_8 + x_9$. We choose $n = 9$ as an illustration because it is convenient for visualizing the attractor structure while maintaining symmetry in this way. The Kaplan-Yorke dimension D_{KY} is calculated from the Lyapunov spectrum, and the result is shown in the middle right panel of Fig. 2. D_{KY} is 2.5, at most, throughout the chaotic region, which justifies the three-dimensional representation of the attractors. The fixed point attractor ($\gamma = 0.925$) [26] becomes saddles, and the attractor becomes a torus ($\gamma = 0.943$) connecting these saddles. To illustrate the structure of the strange attractor in the chaotic region, we first show the torus attractor at the left onset of chaos in Fig. 3. The three-dimensional representation of the attractor is the same as that in the top and bottom panels of Fig. 2. The periodic trajectory travels around nine saddles

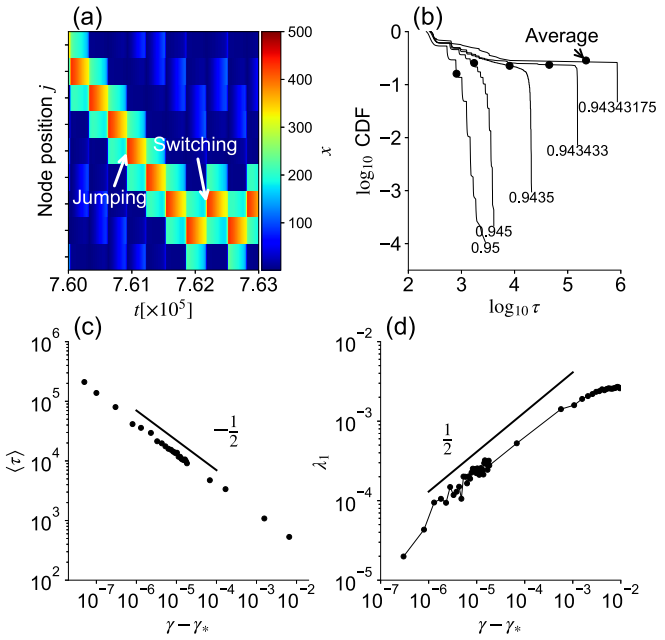


FIG. 4. Summary of the intermittent feature at the onset of chaos. For $\gamma < \gamma_* = 0.9434317$, two periodic attractors traveling in opposite directions exist, as shown in Fig. 3. At the onset of chaos $\gamma \approx \gamma_*$, we found the intermittent switching of the traveling direction. (a) Trajectory at $\gamma = 0.94343175$, slightly above γ_*, represented as a spatiotemporal plot, as in Fig. 1. The terms "jumping" of peak position and "switching" of jumping direction are annotated. (b) Distribution of switching duration τ, measured from a single 10^7 time-unit trajectory. (c) Average of switching duration. (d) Largest Lyapunov exponents λ_1. Here, the Lyapunov exponent is calculated over a 10^6 time-unit trajectory after a 10^6 time-unit transient. The scalings of $\langle\tau$ and λ_1 found here are frequently reported in the intermittency route to chaos.

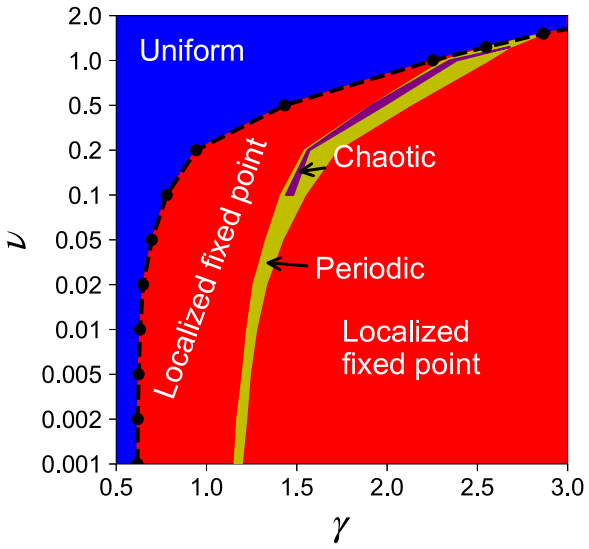


FIG. 5. Phase diagram of the model on a ring with $n = 7$ nodes. Note that Figs. 1–4 are the results for ring $n = 9$ with $\nu = 0.01$. The black dashed lines indicate the bifurcation point of the uniform state, which is analytically derived in Ref. [18]. For small and large ν values, such as 0.001 and 2.0, the chaotic region disappears. The chaotic region does not even exist outside of the range of γ in this figure.

labeled 1, 2, . . ., 9, in that order. This behavior is similar to that of the replicator dynamics, in which invariant subspaces of the model induce structurally stable heteroclinic cycles [27–29]. One difference is the time spent near the saddles, which is linearly increasing for heteroclinic cycles [30], whereas it is constant in our case. Note that the two one-dimensional torus attractors traveling in two directions coexist by reflection symmetry. For a slightly larger value of γ, we obtained a strange attractor by merging these two tori ($\gamma = 0.9445$). At the onset of chaos ($\gamma = \gamma^* = 0.9434317$), switching traveling direction occurs intermittently. The statistics are summarized in Fig. 4. The average duration of switching traveling directions [Fig. 4(c)] and the largest Lyapunov exponent [Fig. 4(d)] support the common scaling law reported in standard literature of intermittency [31,32]. This strongly suggests an intermittency route to chaos in this system.

Once such a strange attractor has been formed, it becomes thick ($\gamma = 0.95$). A region exists near $\gamma = 1$ where the attractor becomes a torus again, connecting nine saddle points of different orders from $\gamma = 0.943$. For a larger γ, a region of chaos exists, again, where the attractor is fully developed [$\gamma = 1.015$; see Fig. 1(c) for the spatiotemporal plot]. As γ reaches the right onset of chaos, the attractor changes form ($\gamma = 1.023$). In this region, the saddle points differ from those observed in $\gamma = 0.943$ and $\gamma = 1.0$ cases. At the right onset of chaos, the saddle points found in $\gamma = 1.023$ stabilize, and the state is in the second localized phase.

We have discussed chaos in the $n = 9$ ring with fixed dissipation $\nu = 0.01$. A similar analysis was performed, as shown in Fig. 2, for rings of different sizes and different values of ν, and it was found that the minimum number of nodes that exihibit chaos is 7, in the case of a ring. The rings with nodes $n \leqslant 6$ did not exhibit chaotic or periodic solutions. The phase diagram of the model (4) for the $n = 7$ ring is shown in Fig. 5. Four regions exist; the uniform state (blue region in Fig. 5), which is identical to the "diffusive phase" in large networks [17], two regions of localized fixed points (red region in Fig. 5), where the localized pattern stablilizes itself, and the periodic [yellow region in Fig. 5) and chaotic regions (purple region in Fig. 5), where the localized patterns are moving regularly or irregularly. One finding is that chaos exists only at intermediate dissipation values ν, approximately between 0.1 and 1.0. One possible mechanism is as follows: For a sufficiently large dissipation, the dynamics are dominated by external interactions; thus, the uniform state can be stable for high γ. The localization wavelength immediately after the bifurcation of the uniform state is sufficiently short, so the localized pattern can be stable. For a sufficiently small dissipation, the peak of the localized pattern has almost every size. The remaining nodes are so small that no driving forces destabilizing the pattern exist.

V. DISCUSSIONS

Our analysis shows that the gravity law transport model exhibits chaos in the ring topology, without any heterogeneity of the parameters or complex network topologies. In partic-

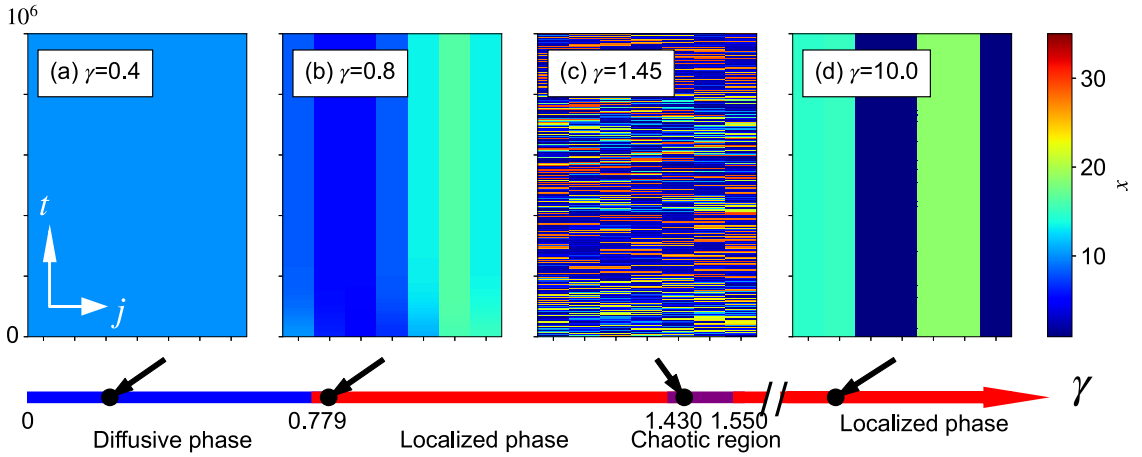


FIG. 6. Typical four phases in the $n = 7$ ring. See Fig. 1 in the main text for a description of the figure.

ular, the chaotic region is found in the localized phase, and the system exhibits low-dimensional chaos after the traveling wavelike periodic solution connecting the saddles, owing to the intermittency of the change in traveling direction. We focused on ring topology in this paper to address the minimality of systems with chaotic behavior, but we have confirmed that chaotic solutions are observed on other network topologies, such as random regular networks. These results may be relevant to chaos in social sciences and economics [33–37]. Our results could be a bridge between separately discussed subjects in socioeconomic systems, namely, gravity law and chaos. Our results highlight several open problems. First, a natural question is the minimal degrees of freedom that exhibit chaos for any network topology, as mentioned previously. We confirmed that none of the strongly connected graphs with four and five nodes exhibit chaotic behaviors. We found chaos in seven-node rings but not in six-node or less (see Appendix). This minimum number may be related to the dominated wavelength of the model, but the detailed mechanism of chaos in this model should be investigated.

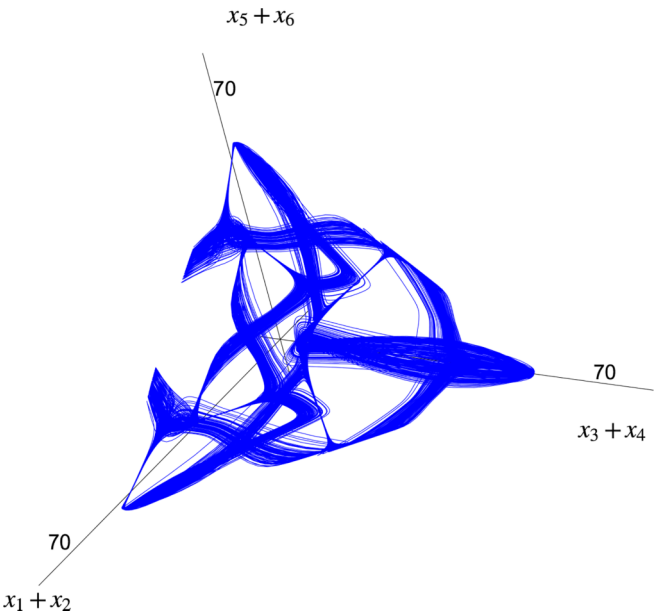


FIG. 7. Attractor structure at $\gamma = 1.45$, $\nu = 0.1$. The attractor is obtained from the 10^5 time-unit trajectory.

Another open problem is the behavior of the large systems, as in reality. In our case, ring topology exhibits chaos with the intermittent change in traveling direction, but other network topologies may exhibit different types of chaotic solutions, which may be more complicated. It would also be interesting to study the behavior of the heterogeneous version of our model, for instance, by introducing link weights, distributed dissipation, and a complex functional form of nonlinearity. For example, link weights can be useful for capturing the role of distances. The role of such heterogeneity in the stability of a system is key to understanding the stability of real systems. Last but not least, the gravity interaction model successfully reproduced the distribution of company sales [17] using the real business network and the parameters estimated from real money flow data. More data collection and analysis of real systems to explore the potential applications of nonlinear transport, along with model studies, are greatly needed for a better understanding of this ubiquitous phenomenon. Our model suggests the possibility that money flow may fluctuate in an economy consisting of companies or countries connected by gravity law. While empirical detection of such chaotic endogenous fluctuations in temporal data presents significant methodological challenges, the identification of these patterns remains a compelling research objective with substantial implications for macroeconomic theory.

ACKNOWLEDGMENTS

This work is supported by a Grant-in-Aid for Scientific Research No. 23KJ0921. H.K. was financially supported by the Japan Society for the Promotion of Science, Research Fellowship for Young Scientists.

APPENDIX: ANALYSIS RESULT FOR $n = 7$ RING

We show that the minimal size for a ring showing a chaotic region is seven in the main text. In this section, we show the

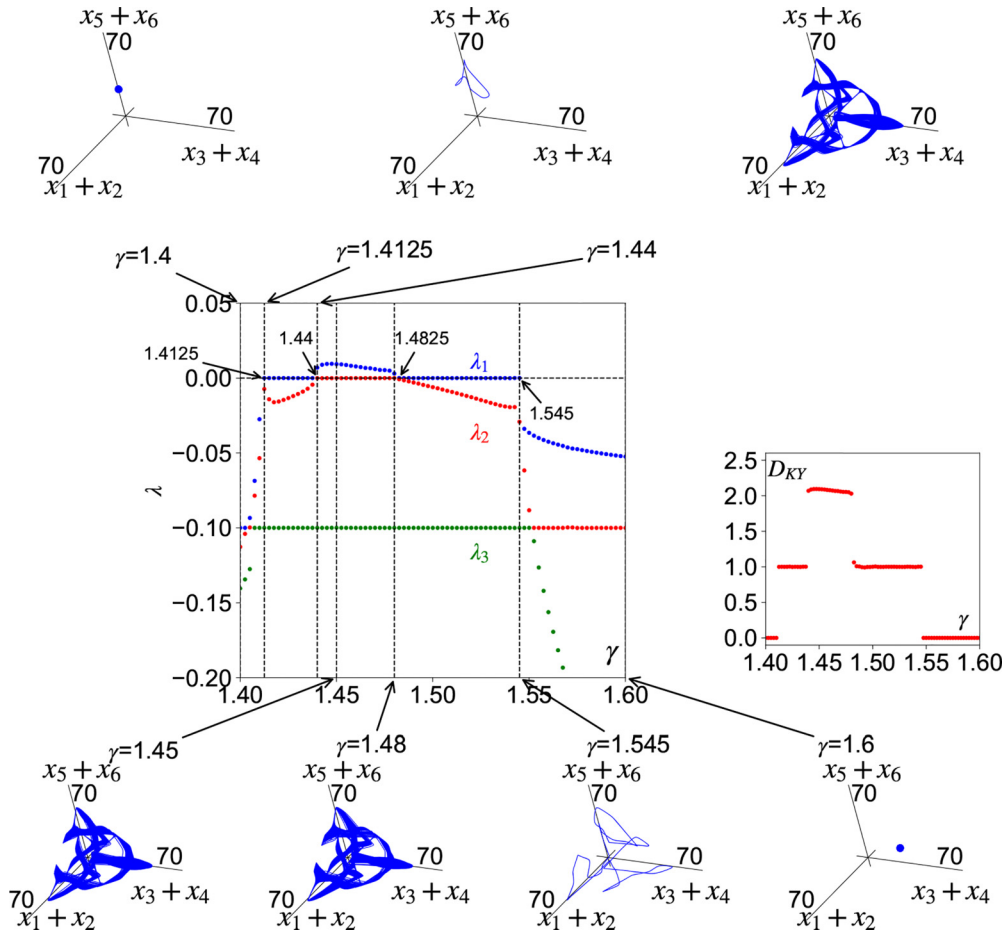


FIG. 8. Lyapunov exponents, Kaplan-Yorke dimension, and attractors. See Fig. 2 in the main text for a description of the figure. For each parameter value, a simulation is performed for the 10^5 time-unit after the 10^3 time-unit transient.

result of analyzing $n = 7$ rings, in parallel to the $n = 9$ result in the main text.

In the case of $n = 7$, the four phases [(a)–(d) in Fig. 1 in the main text] can be seen in the different parameter region for $\nu = 0.1$, as in Fig. 6. In this case, the bifurcation point γ_c is approximately 0.774 for larger $\nu = 0.1$ for $n \to \infty$ ($\gamma_c = 0.576$ in the case $\nu = 0.01$, as seen in the main text). There are four phases, including the chaotic region (limit cycles and chaos), which exists between two localized phases.

The attractor structure for parameter $\gamma = 1.45$, $\nu = 0.1$ on the $n = 7$ ring is then shown in Fig. 7. Simulation is performed for 10^5 time units. Here, three axes—$x_1 + x_2$, $x_3 + x_4$, and $x_5 + x_6$—are chosen because the dynamics, after a sufficiently large transient, are confined in $x_1 + x_2 + x_3 + \cdots + x_7 = \frac{7}{\nu}$ and are thus six-dimensional. Lyapunov exponents and the Kaplan-Yorke dimension confirmed that this three-dimensional representation of the attractor is justified (see Fig. 8).

[1] J. Tinbergen, *Shaping the World Economy: Suggestions for an International Economic Policy* (Twentieth Century Fund, New York, 1962).

[2] J. E. Anderson, The Gravity Model, Annu. Rev. Econ. **3**, 133 (2011).

[3] E. G. Ravenstein, The laws of migration, J. Stat. Soc. London **48**, 167 (1885).

[4] G. K. Zipf, The P 1 P 2 D hypothesis: On the intercity movement of persons, Am. Sociol. Rev. **11**, 677 (1946).

[5] J. J. Lewer and H. V. den Berg, A gravity model of immigration, Econ. Lett. **99**, 164 (2008).

[6] H. J. Park, W. S. Jo, S. H. Lee, and B. J. Kim, Generalized gravity model for human migration, New J. Phys. **20**, 093018 (2018).

[7] R. Prieto Curiel, L. Pappalardo, L. Gabrielli, and S. R. Bishop, Gravity and scaling laws of city to city migration, PLoS ONE **13**, e0199892 (2018).

[8] S. Erlander and N. F. Stewart, *The Gravity Model in Transportation Analysis: Theory and Extensions* (VSP, Utrecht, 1990).

[9] W.-S. Jung, F. Wang, and H. E. Stanley, Gravity model in the Korean highway, Europhys. Lett. **81**, 48005 (2008).

[10] L. Wang, J.-C. Ma, Z.-Q. Jiang, W. Yan, and W.-X. Zhou, Gravity law in the Chinese highway freight transportation networks, EPJ Data Science **8**, 1 (2019).

[11] R. Li, S. Gao, A. Luo, Q. Yao, B. Chen, F. Shang, R. Jiang, and H. E. Stanley, Gravity model in dockless bike-sharing systems within cities, Phys. Rev. E **103**, 012312 (2021).

[12] A. P. Masucci, J. Serras, A. Johansson, and M. Batty, Gravity versus radiation models: on the importance of scale and heterogeneity in commuting flows, Phys. Rev. E **88**, 022812 (2013).

[13] O.-H. Kwon, I. Hong, W.-S. Jung, and H.-H. Jo, Multiple gravity laws for human mobility within cities, EPJ Data Science **12**, 57 (2023).

[14] K. Tamura, W. Miura, M. Takayasu, H. Takayasu, S. Kitajima, and H. Goto, Estimation of flux between interacting nodes on huge inter-firm networks, Int. J. Mod. Phys. Conf. Ser. **16**, 93 (2012).

[15] H. Wang, X.-Y. Yan, and J. Wu, Free utility model for explaining the social gravity law, J. Stat. Mech. (2021) 033418.

[16] J. de Dios Ortúzar and L. G. Willumsen, *Modelling Transport* (John Wiley & Sons, Inc., Hoboken, NJ, 2024).

[17] K. Tamura, H. Takayasu, and M. Takayasu, Diffusion-localization transition caused by nonlinear transport on complex networks, Sci. Rep. **8**, 5517 (2018).

[18] H. Koike, H. Takayasu, and M. Takayasu, Diffusion-localization transition point of gravity type transport model on regular ring lattices and Bethe lattices, J. Stat. Phys. **186**, 44 (2022).

[19] H. Koike, H. Takayasu, and M. Takayasu, Bifurcation and hysteresis in a nonlinear transport model on network motifs, Phys. Rev. Res. **6**, 013059 (2024).

[20] E. Viegas, O. Levy, S. Havlin, H. Takayasu, and M. Takayasu, Spatial constraints on economic interactions: A complexity approach to the Japanese Inter-Firm Trade Network, Mathematics **12**, 1244 (2024).

[21] M. Karpiarz, P. Fronczak, and A. Fronczak, International trade network: Fractal properties and globalization puzzle, Phys. Rev. Lett. **113**, 248701 (2014).

[22] J. E. Anderson and E. van Wincoop, Gravity with gravitas: a solution to the border puzzle, Am. Econ. Rev. **93**, 170 (2003).

[23] K. Tamura, H. Takayasu, and M. Takayasu, Extraction of conjugate main-stream structures from a complex network flow, Phys. Rev. E **91**, 042815 (2015).

[24] See Supplemental Material at http://link.aps.org/supplemental/10.1103/PhysRevResearch.7.023232 for details on the derivation of the dispersion relation, which is based on the eigenvalues of the Jacobian matrix of model (4) at a uniform state [18].

[25] I. Shimada and T. Nagashima, A numerical approach to ergodic problem of dissipative dynamical systems, Prog. Theor. Phys. **61**, 1605 (1979).

[26] Only one fixed point is shown in Fig. 2, but there are other fixed points owing to symmetry.

[27] J. Hofbauer and K. Sigmund, *Evolutionary Games and Population Dynamics* (Cambridge University Press, Cambridge, 1998).

[28] J. Hofbauer and K. Sigmund, *The Theory of Evolution and Dynamical Systems: Mathematical Aspects of Selection* (Cambridge University Press, Cambridge, 1988).

[29] T. Chawanya, A new type of irregular motion in a class of game dynamics systems, Prog. Theor. Phys. **94**, 163 (1995).

[30] R. M. May and W. J. Leonard, Nonlinear aspects of competition between three species, SIAM J. Appl. Math. **29**, 243 (1975).

[31] Y. Pomeau and P. Manneville, Intermittent transition to turbulence in dissipative dynamical systems, Commun. Math. Phys. **74**, 189 (1980).

[32] S. Elaskar and E. del Río, Review of chaotic intermittency, Symmetry **15**, 1195 (2023).

[33] T. Puu, *Nonlinear Economic Dynamics* (Springer, Berlin, Heidelberg, 1991).

[34] T. Puu, *Attractors, Bifurcations, & Chaos: Nonlinear Phenomena in Economics* (Springer, Berlin, New York, 2013).

[35] W. A. Barnett, A. Serletis, and D. Serletis, Nonlinear and complex dynamics in economics, Macroeconomic Dynamics **19**, 1749 (2015).

[36] M. San Miguel and R. Toral, Introduction to the chaos focus issue on the dynamics of social systems, Chaos **30**, 120401 (2020).

[37] T. J. Gordon, Chaos in social systems, Technol. Forecasting Social Change **42**, 1 (1992).